Phonons in semiconductor planar microcavities: A Raman scattering study

A. Fainstein and B. Jusserand
France Telecom, Centre National d'Etudes des Télécommunications, PAB-Laboratoire de Bagneux, Boîte Postale 107, 92225 Bagneux Cedex, France
(Received 22 May 1996)

We present a detailed Raman-scattering study of optical and folded-acoustic phonons in semiconductor planar microcavities. The GaAs-like optical-phonon Raman spectra consists of a series of peaks due to the microcavity ''interface-phonon'' band, comprising both distributed Bragg reflector and embedded quantum-well modes. Finite-size effects are shown, including the observation of surface vibrations, wave-vector quantization leading to a discretization of the interface-mode bands, and relaxation of the conservation of the latter in scattering processes. Phonon energies, their in-plane mode dispersion, and Raman-scattering selection rules can be well accounted for by symmetry considerations and calculations of the phonon spectra and electrostatic potentials based on a dielectric continuum model. A further doubling of the folded acoustic-phonon Raman peaks is observed in a multiple-quantum-well filled microcavity, demonstrating the presence of forward-scattering processes in backscattering geometries with Bragg mirrors. These results highlight the potentialities of Raman scattering as a material sensitive tool to access the photon mode structure of photonic devices. [S0163-1829(96)05640-8]

I. INTRODUCTION

Electromagnetic excitations of layered semiconductors, and their scattering by light, have attracted considerable attention in the last 10–15 years, caused by the technological ability to grow such structures by epitaxial techniques with almost steplike interfaces.[1,2] The modification of the long-range Coulomb forces due to the presence of planar boundary conditions qualitatively changes the properties of both phonons and plasmons. In addition, these modified phonon and plasmon excitations may coexist, in different length scales, with another two consequences of the layering: electron and photon confinement. The first exists when the carriers are confined in their movement to sizes of the order of their de Broglie wavelength. The latter, on the other hand, can be tailored to appear in structures with larger characteristic thicknesses, typically of the order of the light wavelength. Such optical microcavities, which are the subject of this paper, can in fact be made by enclosing a spacer layer between two distributed Bragg reflectors.

Following work done in the domain of atomic physics,[3] research on semiconductor microcavities found a strong impulse in recent years in view of their rich physics and numerous possible applications in optoelectronic devices.[4] It has been realized for some time that the radiation properties of matter may be modified not only by tailoring its electronic structure but also by monitoring the radiation field itself. In fact, the light field in the vicinity of an atom can be altered, e.g., by placing it near a surface[5] or within a microcavity[3,4] or a photonic band-gap material.[6] These modifications of the photon electric fields can be exploited in both first order in light-matter interaction processes: absorption *and/or* emission.[7] Likewise, and by modification of each or both of its two vertexes of light-matter interaction, the inelastic-scattering cross-section of an active material can also be strongly enhanced or inhibited.[8–12]

We have recently reported on the observation of a dramatic enhancement (over four orders of magnitude) of the Raman signals in a GaAs/AlAs-based monolithic semiconductor planar microcavity.[11] In Ref. 11 we described GaAs-like optical-phonon Raman scattering in photon field confinement conditions for a $\lambda/2$ AlAs cavity made of GaAs/AlAs mirrors, with two $In_xGa_{1-x}As$ quantum wells (QW's) embedded at its core. The spectra observed in the GaAs optical-phonon frequency region consists of a complex series of peaks, which we suggested to be due to scattering by the microcavity interfacelike modes, discretized by finite-size effects. In this paper we present a comprehensive study of the optical-phonon spectra of such structures. The observed interface modes are always present in a semiconductor cavity, independently of the specific active medium embedded at its core, and thus their detailed understanding is a key step toward using Raman spectroscopy to study weakly scattering objects in cavity geometries. In addition, a quantitative analysis of the spectra may serve to monitor the field distribution within these structures. We will not dwell much on the question of enhancement by optical confinement, which was the topic of Refs. 11 and 12, but rather deepen the description of the Raman spectra. We have extended our previous experimental results to other microstructures. Results for both full and half cavities are presented, which clearly demonstrate our assignment of the spectra to interfacelike optical phonons modified by finite-size effects. In addition, we present results for structures in which the spacer is made of a material different to those making the mirrors, to resolve spectrally their contribution to the Raman signal. We discuss the mode frequencies, their in-plane dispersion, and the Raman selection rules in terms of symmetry considerations and a dielectric continuum model for the optical vibrations in these nonperiodic layered structures. This model has the advantage of an extreme simplicity, while giving a reasonable description of the data which can be later improved by more sophisticated approaches. Finally, folded-acoustic-phonon spectra are briefly presented. A doubling of the spectra

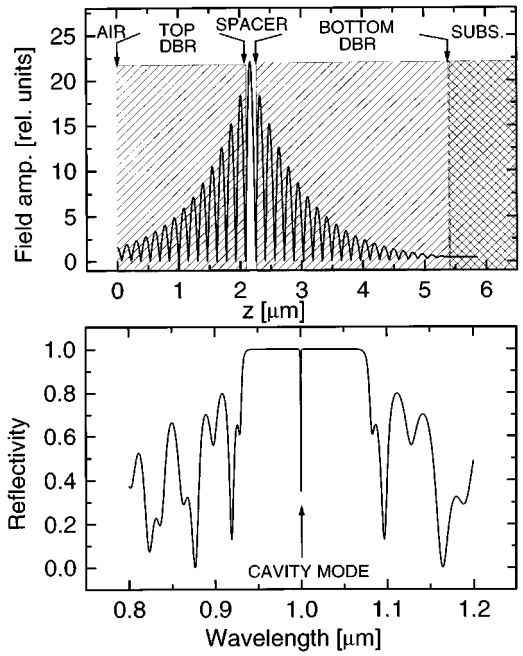

FIG. 1. Reflectivity (bottom) and cavity-mode electric-field distribution (top) for a λ/2 AlAs cavity enclosed by GaAs/AlAs quarter-wavelength layers, 20 pairs below, 13.5 above, and grown over a GaAs substrate. The layer thicknesses are normalized for cavity resonance at $\lambda = 1\,\mu$m.

clearly demonstrates the presence of both backscattering and forward-scattering processes in cavity geometries.

The paper is organized as follows. In Sec. II we present a theoretical overview which will help to discuss the experimental results. The samples and experimental setup are described in Sec. III, and our experimental results and analysis follow in Sec. IV. Finally, conclusions are drawn in Sec. V.

II. THEORETICAL OVERVIEW

A. Optical confinement in semiconductor planar microcavities

As commented in Sec. I, in a planar microcavity both the optical and vibrational modes reflect the samples layered structure. We begin by briefly describing the photon field confinement and how this influences the Raman scattering efficiency in such a structure. The phonon interfacelike modes are the subject of the last part of this overview.

Dielectric mirrors (with reflectivity larger than 99%) are obtained by depositing alternatively quarter-wave layers of materials of different refractive index. These layered structures, so-called distributed Bragg reflectors (DBR's), display a stopband with energy width and reflectivity depending on the contrast of indices and the number of periods, respectively. A microcavity, obtained by growing a variable-width center layer (spacer), introduces a ''photon impurity state'' within this one-dimensional photonic band gap, for which light is transmitted throughout the structure and its electric field partially confined and enhanced within it.[13]

In Fig. 1 we show the reflectivity and electric-field distribution for normal incidence (along the cavity axis z) on a λ/2 AlAs cavity with GaAs/AlAs DBR's, 20 pairs below, and 13.5 above, and grown over a GaAs substrate. The curves were calculated using the standard method of matrices.[14] The field distribution corresponds to the vertical cavity mode, and is normalized to the incident amplitude. Note that it is enhanced throughout the whole microstructure, displaying a maximum of about 20 at the center. On the other hand, if the spacer is removed leaving only the quarter wavelength layers of the DBR's, or if the photon frequency is detuned from the cavity mode, the electric field decays exponentially into the mirror and no enhancement is observed.

B. Optical double-resonant Raman scattering

The above-described spectrally dependent modifications of the photon field amplitude and spatial distribution can be exploited to produce enhanced Raman signals in planar semiconductor microcavities.[11,12] High finesse cavities, as required for maximum field enhancement, are obtained by the use of almost total reflectivity mirrors. Thus, in Raman-scattering experiments performed on the face normal to the growth (z) axis of such a structure, both the incoming and outgoing photons (separated by the energy of the excitation under study, e.g., 36 meV for a GaAs optical phonon) must resonate with optical modes of the cavity in order to get into, or go out from, the structure. For a planar semiconductor microcavity with a single vertical mode, this can be accomplished by taking advantage of the continuum of in-plane optical modes.[11] In fact, if ω_0 is the frequency of the cavity mode along z, and $k_\parallel$ the photon in-plane wave vector, the mode dispersion is given by

$$\omega(k_\parallel) = \sqrt{\omega_0^2 + (ck_\parallel / n_{\text{eff}})^2}. \tag{1}$$

An optical double resonance can hence be achieved by tuning the angle (respect to z) between incoming and scattered rays.[11] For example, if light is collected along z, the required incidence angle θ_o (measured in air) for Stokes scattering of an excitation of frequency ω_{ph} will be given approximately by

$$\theta_o \approx n_{\text{eff}} \arccos\left(\frac{\omega_0}{\omega_0 + \omega_{\text{ph}}}\right). \tag{2}$$

Here n_{eff} is an effective refractive index for the cavity.

In principle *both* the excitation and collection directions may be varied according to Eq. (1). In-plane dispersions can be thus derived by changing the wave vector transferred in the scattering process. Also, both Stokes and anti-Stokes (i.e., emission or absorption of an excitation by the incoming photon, respectively) configurations are feasible, depending on whether the excitation or the scattered light angle is the largest.

In order to understand how these cavity modifications of the photon fields influences inelastic scattering, let us present the following expression for the third-order optical-phonon resonant Raman-scattering efficiency (second order in light-matter and first order in electron-phonon interaction):[15]

$$\sigma(\omega) \propto \left| \sum_{ij} \frac{\langle f|H_{\text{MR}}|j\rangle\langle j|H_{e\text{-ph}}|i\rangle\langle i|H_{\text{MR}}|0\rangle}{(\omega - \omega_i - i\gamma_i)(\omega - \omega_j - i\gamma_j)} \right|^2, \tag{3}$$

where $|0\rangle(|f\rangle)$ denotes the initial (final) state of the scattering process, and $|i\rangle(|j\rangle)$ are intermediate excitonic states

with transition energies and lifetime broadening given by $\omega_i(\omega_j)$ and $\gamma_i(\gamma_j)$. In Eq. (3) $H_{e\text{-ph}}$ describes the appropriate electron-phonon interaction (e.g., deformation potential or Fröhlich),[1,15] while H_{MR} corresponds to the radiation-matter Hamiltonian. There are two matrix elements of H_{MR} due to the incoming and outgoing photon vertexes. These are proportional to the electric-field amplitude of the incident and scattered photons, respectively.

Equation (3) shows that simple or double *optical* resonances of the Raman efficiency exist if the incident or scattered photons or both are resonant with the *photonic* quantized levels of the microcavity. In the case of a double resonance, the Raman-scattering efficiency is *fourth order* in the cavity-field enhancement factor. Note that the Raman efficiency is not only sensible to the spectral dependence of the photon modes of the cavity, but also to their electric-field spatial distribution. This ''optical resonant Raman scattering'' may be paralleled with the more familiar *electronic* resonance processes:[15] due to the resonant denominators in Eq. (3), incoming, outgoing, or double *electronic* resonances exist depending on whether the incident, scattered, or both photons, respectively, are resonant with *excitonic* transitions in the material.

In Ref. 12 we showed that a quantitative description of the Raman efficiency modifications in a semiconductor microcavity can be obtained by simply taking into account the separate contribution (i.e., the product) of the purely electromagnetic enhancement of the excitation and emission steps in the scattering process. This contrasts with the usual case in surface-enhanced Raman scattering,[9,16] where the coupling to *mirror* electronic resonances provides the largest enhancement mechanism. This relative simplicity of the DBR microcavities, where no energy transfer to the mirrors occurs, will prove useful in order to describe nonlinear optical phenomena under optical confinement.

C. Interfacelike optical-phonon modes in layered media

Let us now describe the excitations which will be the main subject of our present study, i.e., the optical vibrations of the layered structure consisting of the microcavity and, eventually, some QW's embedded at its core. The collective excitations of layered polar dielectric materials, both electronic and vibrational, have been extensively discussed in the past.[1,2,17–28] In particular, simple dielectric continuum models,[17] modified dielectric continuum models which take into account mechanical boundary conditions besides the electrostatic ones,[18] and microscopic calculations[19,20] have been reported for the description of the optical vibrations.

References 1, 2, and 17–20 describe periodic infinite structures. In addition, single slabs,[21,22] *finite* (but otherwise periodic) structures,[23–25] and light scattering by plasmons in the latter,[26–28] have been also discussed within the simpler dielectric continuum models. Finite-size effects may be basically resumed in the apparition of ''surface modes'' at the limiting surfaces of the sample, and in a discretization of the wave vector along the heterostructure symmetry axis. Also, a relaxation of the wave-vector conservation along the growth axis is expected in a scattering process. In fact, such effects have been observed in the case of plasmons by Pinczuk, Lamont, and Gossard.[28] On the other hand, experiments in single layers have been reported which demonstrated the existence of surface vibrations.[21,22]

The evaluation of the optical-phonon modes in a microcavity is comparatively more complicated in that it is a nonperiodic massive layered structure, and thus no simple analytic expressions for the phonon dispersions are obtainable. We have thus calculated the optical-phonon modes extending the usual dielectric continuum model[23] by the use of a matrix method closely related to that used to describe the propagation of light in layered media.[14] This method, specially suitable for heterostructures with an arbitrary sequence of layers, will be briefly described next.

Lattice motions create an electric field which may be expressed (in the absence of retardation) in terms of a scalar potential ϕ. For a layered system, with z its axis and isotropic in the xy plane, this potential should be of the form $\phi(\vec{r})=\phi(z)\exp(iq_{\parallel}r_{\parallel})$ and satisfy[23]

$$\epsilon(\omega)\left[\frac{\partial^2\phi(z)}{\partial z}-q_{\parallel}^2\right]=0, \tag{4}$$

where $\epsilon(\omega)$ is the dielectric function of the medium (different for each layer), and $q_{\parallel}$ is an in-plane wave vector. As usual, the dielectric function of each material is taken as $\epsilon_j=\epsilon_{\infty j}(\omega_{Lj}^2-\omega^2)/(\omega_{Tj}^2-\omega^2)$, with ω_{Lj} and ω_{Tj} the LO (longitudinal optical) and TO (transverse optical) frequencies, respectively, and $\epsilon_{\infty j}$ the high-frequency dielectric constant of material j. For the frequencies which correspond to zeros of $\epsilon(\omega)$, the modes result bulklike and confined to each layer.[23] More interesting here are those modes for which $\epsilon(\omega)\neq 0$, which are extended modes specific of the layered system. These vibrations are conventionally termed interface modes.[29]

The problem consists hence in finding solutions to Eq. (4), in an arbitrary layered material, and subject to the boundary conditions that require continuity of ϕ and of the normal component of the field displacement at the interfaces. In addition, the localization of ϕ in space is required, i.e., that the potential should be zero at $\pm\infty$. We note here that we do not take into account mechanical boundary conditions at the interfaces, which are known to be important to correctly describe the coupling of ''interface'' and confined phonon modes in thin QW's.[18] The layers making our structures are usually relatively thick, and hence phonon confinement effects are not expected to be important.

For the electrostatic potential within layer n, defined by $z_n\leqslant z\leqslant z_{n+1}$, we take the general form

$$\phi(z)=a_n\exp q_{\parallel}(z-z_n)+b_n\exp -q_{\parallel}(z-z_n). \tag{5}$$

The coefficients a_n and b_n in layer n, expressed as a two-component vector, can be related with those in layer $n+1$ by multiplication of the latter by the following ''transfer'' matrix derived by application of the boundary conditions to Eq. (5):

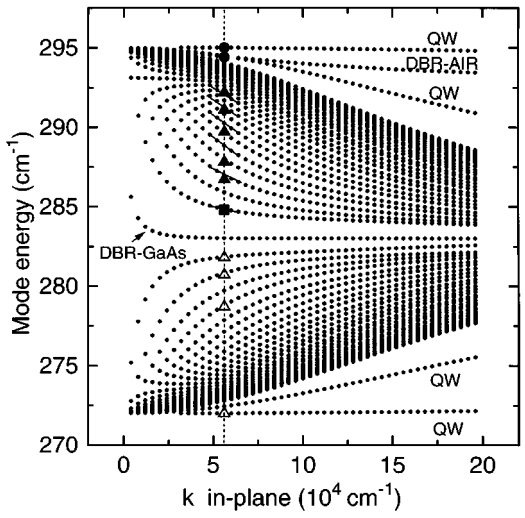

FIG. 2. Interface-phonon dispersion (small dots) as a function of in-plane wave vector $q_\parallel$ calculated for the finite heterostructure consisting of a bottom and a top GaAs/AlAs DBR (20 and 13.5 pairs, respectively) enclosing an AlAs $\lambda/2$ cavity, with, in addition, two $In_{0.14}Ga_{0.86}As$ QW's at its center (modeled as GaAs layers; see text for details). The structure is limited above by air and below by the GaAs substrate. The vertical dashed line denotes the experimental transferred $q_\parallel$. Symbols correspond to the experimental points. The short solid lines indicate the modes which are allowed to scatter due to parity.

$$T_{n,n+1} = \frac{1}{2}\begin{pmatrix} \left(1+\frac{\epsilon_{n+1}}{\epsilon_n}\right)\exp -q_\parallel d_n & \left(1-\frac{\epsilon_{n+1}}{\epsilon_n}\right)\exp -q_\parallel d_n \\ \left(1-\frac{\epsilon_{n+1}}{\epsilon_n}\right)\exp q_\parallel d_n & \left(1+\frac{\epsilon_{n+1}}{\epsilon_n}\right)\exp q_\parallel d_n \end{pmatrix}, \tag{6}$$

where ϵ_n is the dielectric function of layer n, and d_n its thickness. The coefficients of the first (0, e.g., *air*) and last (N, e.g., *substrate*) layers can hence be related by the closed relation

$$\begin{pmatrix} a_0 \\ b_0 \end{pmatrix} = T\begin{pmatrix} a_N \\ b_N \end{pmatrix}, \tag{7}$$

where T is simply the matrix product of the $N-1$ transfer matrices [Eq. (6)] defined by the structure. By further noting that, due to the localization of the potential, a_N and b_0 must be zero, we find the implicit equation

$$T_{22} = 0, \tag{8}$$

which is solvable numerically for the eigenfrequencies of the interfacelike modes of the structure. Once the eigenfrequencies are obtained, the potential at each layer can be calculated in terms of the normalization constant b_N by using Eq. (5) with the respective coefficients obtained by succesive application of the transfer matrix Eq. (6). Finally, the normalization coefficient may be determined from energy considerations once the potential has been evaluated.

In Fig. 2 we show the calculated phonon dispersion in the GaAs range and as a function of the in-plane wave vector

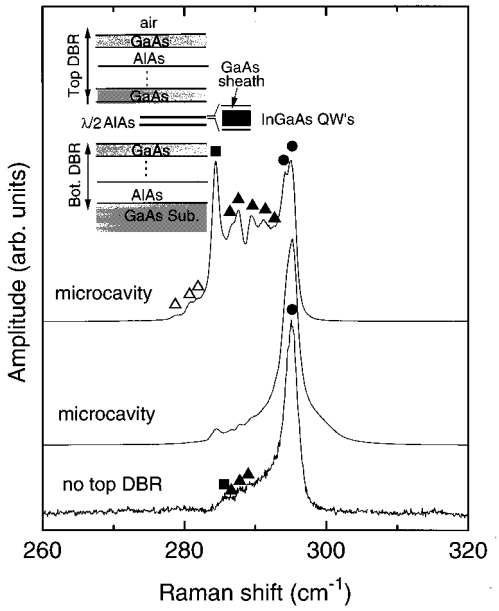

FIG. 3. GaAs-like optical-phonon Raman spectra taken with the $z'(x,y)\bar{z}$ configuration for both the AlAs-cavity and test (without top DBR) samples. The laser energy was 1.35 eV, incident at 54° respect to z (external to the sample). Stokes photons are collected along z. θ_0 was tuned for cavity optical double resonance slightly below the LO peak ≈ 295 cm^{-1}. The two AlAs-cavity spectra (top curves) correspond to different spot positions on the wafer, i.e., selective enhancement of different Stokes regions. The same symbols used to label the peaks are shown as experimental points in Fig. 2. The amplitude of the spectra are normalized. A sketch of the cavity sample is shown as an inset.

$q_\parallel$ (small dots) for the cavity structure described in Fig. 1 with, in addition, two 14-nm GaAs QW's (separated by 3 nm) embedded at the center of the AlAs spacer. This structure is schematized in the inset of Fig. 3. One mode is observed for each interface, contributing to two almost continuous bands plus other clearly separated branches.[23] It is possible to relate these modes to specific regions in the heterostructure, i.e., the surfaces limiting the DBR's, the DBR's themselves, or the central QW's, by evaluating their associated electrostatic potential. This assignment (shown for identification purposes in Fig. 2) is essentially correct for large in-plane wave vectors. In a Raman-scattering experiment with infrared light and for the geometry we will discuss, $q_\parallel \leqslant 6\times 10^{-4}$ cm^{-1}. For this relatively small value, the vibrations are not completely localized, but tend to be extended throughout the structure. Examples of these potentials will be shown below when discussing the experimental results. The so-called ''finite-size'' effects are apparent in the phonon dispersion in Fig. 2. Besides the existence of separate modes related to surface states, each discrete curve in the DBR bands corresponds to a different quantized wave vector along z: if D and d are the total size of the structure and the DBR's period, respectively, for the upper DBR band q_z ranges from the smallest value (π/D) at the bottom to the largest possible one (π/d) at the top. Note, for comparison, that in an infinite layered structure the interface modes form two *continuous* bands corresponding to $0<q_z<\pi/d$.[1,2] These bands, characteristic of layered media, reflect the

strong anisotropy introduced by the boundary conditions on the Coulomb polarization fields. In fact, Fig. 2 shows that, for the calculated structure, the LO-TO splitting reduces to half its value for in-plane propagation. This can be understood through a handwaving argument as follows: for a GaAs-like vibration only the GaAs layers are polarized, leading for an in-plane longitudinal mode in a GaAs/AlAs (50%/50%) heterostructure to only *half* the restoring electrostatic force found in bulk.

III. SAMPLES AND EXPERIMENTAL SETUP

We have made a comprehensive study of phonon Raman scattering in a series of molecular-beam-epitaxy-grown microcavities. Of these, we will present here results selected to better highlight different aspects of the phonon spectra in these layered structures. Two groups of samples, comprising two cavities each, will be discussed. One cavity of the first group (from now on ''AlAs''-cavity),[30] consists of a 20-pair AlAs/GaAs bottom DBR grown on a GaAs substrate, followed by a half-wave AlAs spacer which constitutes the body of the cavity, and finally 13.5 pairs of GaAs/AlAs forming the top Bragg mirror. Two 12-nm-wide strained $In_{0.14}Ga_{0.86}As$ quantum wells are located at the center of the AlAs cavity, and separated by a center-to-center distance of 17 nm. For growth quality reasons, each quantum well is enclosed on either side by a 1-nm-wide layer of GaAs. The optical-field modifications and GaAs-like interface-phonon dispersion of this cavity were presented in Figs. 1 and 2. For comparison, a second ''test-AlAs'' sample identical to the AlAs cavity but with its growth stopped just after the AlAs spacer (i.e., without top DBR) was also studied.

A second group of microcavities was made with the aim of clearly separating the contributions to the Raman spectra coming from spacer and DBR's. Both a cavity structure (from now on a ''MQW'' cavity) (MQW is a multiple quantum well) and its partner test sample (i.e., without the top DBR, from now on ''test-MQW'' cavity) were studied. The spacer, of total thickness $3\lambda/2$, consists of 36 periods of GaAs/AlAs (70 Å/30 Å) MQW, enclosed above by 25 periods and below by 28 periods of $Al_{0.33}Ga_{0.67}As$/AlAs quarter-wavelength layers acting as DBR's. Again, the samples are grown on GaAs substrates. The layers thickness in all four samples is largest at the center of the wafer and decreases by $\approx 20\%$ over the 1-in. radius of the wafer, enabling the tuning of the cavity mode by displacing radially the spot under examination.[11]

Raman scattering experiments were performed at 77 K, with a DILOR-XY800 multichannel Raman setup. For Stokes scattering experiments the scattered radiation was collected (with a $f/2$ aperture) along or close to the axis of the cavity (z), while the incident laser angle was correspondingly tuned for double optical resonance.[11] Anti-Stokes experiments were also performed on the MQW cavity. In this case the incidence and collection angles (and also their photon energies) are reversed respect to the Stokes geometry. Although the signals are less intense for the anti-Stokes case, we found it more convenient to derive in-plane dispersions under optical resonant conditions.

IV. RESULTS AND DISCUSSION

A. Finite-size effects

We start by presenting data on GaAs-like optical-phonon scattering on both the AlAs and test-AlAs cavities. First we limit our discussion to the frequencies of the observed modes, pointing out those features which derive from the so-called ''finite-size effects.'' Raman-scattering selection rules, in-plane dispersions, and folded acoustic-phonon scattering will be discussed in following subsections.

In Fig. 3 we show Raman spectra of both the cavity and test ''AlAs'' samples, for a crossed $z'(x,y)\bar{z}$ configuration with an excitation energy of 1.35 eV (well below the QW gap ≈ 1.385 eV). Although the inelastic-scattering signals are strongly amplified in the cavity sample (over four orders of magnitude respect to the test sample[11]), we found that Raman experiments must be performed below the QW gap in order to avoid the exciton luminescence that is also enhanced several orders of magnitude due to optical confinement. As usual, $x(y)$ indicates incident (scattered) light polarized along the crystal axis (100) [(010)], and $\bar{z}$ a scattered photon propagating along z. With z' we indicate light incident not normal to the cavity but, for this case, at 54° (external) with respect to z. The spectra in Fig. 3 were taken with the incident angle tuned for optical double-resonant Stokes scattering by phonons of frequency slightly below that of the longitudinal optical-phonon of GaAs ($LO \approx 295\ cm^{-1}$). The two full-cavity spectra differ in their spot positions in the wafer (0.06 mm apart one from the other), so that different regions of the spectra are selectively amplified (see Ref. 11 for details). The latter enables a precise determination of the peak frequencies. The test sample spectrum was taken under exactly the same experimental conditions but due to the reduced scattering efficiency,[11,12] much longer integrations were required (600 s, compared with 1 s for the cavity spectra).

The cavity spectra shown in Fig. 3 display a complex series of peaks, the relative amplitudes of which can be varied by different enhancement conditions. Nevertheless, some general conclusions can be drawn from the data: (i) the Raman spectra appear between the LO and TO ($\approx 272\ cm^{-1}$) frequencies of bulk GaAs; (ii) two bands can be identified according to their intensity, one very strong and delimited above by the LO phonon and below by a second peak at $\approx 285\ cm^{-1}$ (see the solid circles and squares, respectively, on the upper spectrum of Fig. 3), the other much weaker between the latter and the TO frequency; (iii) the most intense peaks occur at the LO phonon and at $\approx 285\ cm^{-1}$, several smaller ones (labeled with full triangles) appearing between them; and finally, (iv) scattering occurs principally for the $z'(x,y)\bar{z}$ configuration.

The test sample spectrum, on the other hand, also displays a main peak located at the bulk-GaAs longitudinal-optical-phonon frequency, with, in addition, some smaller features at lower energies ranging from $\approx 285\ cm^{-1}$ to the LO energy. Note, however, that the Raman shifts of these secondary peaks are *not* exactly the same for the two samples. Most notably, the lower-frequency peak in the test sample spectrum (labeled with a solid square) appears at an energy clearly *above* that of the respective peak in the cavity structure.

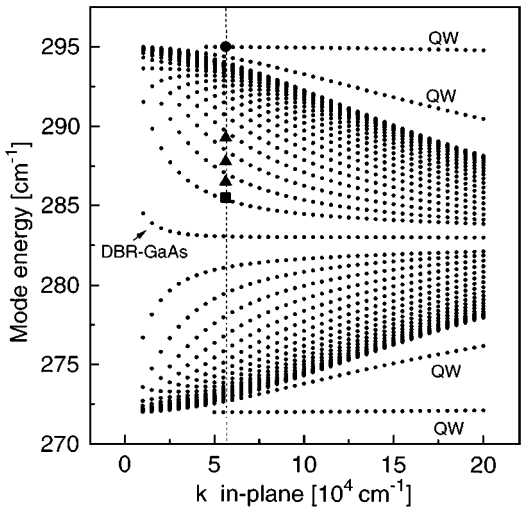

FIG. 4. Interface-phonon dispersion (small dots) as a function of in-plane wave vector $q_\parallel$ calculated for the test-AlAs cavity, i.e., a structure similar to the one represented in Fig. 2 but *without* top DBR. The vertical dashed line denotes the experimental transferred $q_\parallel$. The experimental points are labeled, for clarity, as in Fig. 3.

In Figs. 2 and 4 we compare the calculated GaAs-like interface-phonon dispersion of the two AlAs cavities with the corresponding Raman spectra in Fig. 3. The same symbols shown as experimental points over the dispersion curves are used to label the peaks to facilitate their identification. There is essentially no fitting parameter: the calculated dispersion curves depend only on the layers thickness (nominal values were used) and the TO- and LO-phonon frequencies, here taken from the experiment but otherwise coincident with literature values.[31] We describe the optical phonons of the 12-nm $In_xGa_{1-x}As$ QW's plus their 1-nm GaAs caps as those of 14-nm-thick GaAs slabs. In fact, due to a compensation of the effects of alloying and strain, the zone-center GaAs-like phonons of thin strained $In_xGa_{1-x}As$ layers grown on GaAs resemble almost exactly those of GaAs.[32,33] Note that the transferred in-plane wave vector, shown with a vertical dashed line in Figs. 2 and 4, is uniquely determined by the scattering configuration.

According to Figs. 2 and 4, we assign the main experimental peaks to scattering by the QW's, DBR-air surface and upper DBR-band modes. The experimental peaks within the DBR band (full triangles) are reasonably well accounted for by theory (within 1 cm^{-1}) if one every two modes scatter in the AlAs cavity, a requirement not present for the test sample. We will see below that this is a consequence of a parity selection rule. A similar analysis will lead us to assign the doublet of the cavity LO-like peak (solid circles on the upper spectrum in Fig. 3) to the lower more dispersive QW mode and to the DBR-air surface vibration. Besides the existence of this latter mode, and the discretization of the DBR spectra due to q_z quantization, finite-size effects provide a straightforward explanation for the relative shift of the bottommost mode in the upper DBR band of the two samples (labeled with solid squares). In fact, the different frequencies of these modes is neatly derived in the calculated phonon dispersions. These modes correspond to the smallest quantized q_z, which we recall is given by π/D, with D the total thickness of the cavity. For the full cavity D is larger, hence the minimum q_z is smaller, and thus the corresponding mode frequency is lower. Note that these modes, which propagate almost normal to z (i.e., in plane), are usually not observable in a backscattering configuration.

B. Selection rules

In Sec. IV A, we showed that the spectra observed in the AlAs full and test cavities could be assigned to scattering by interface modes of the whole layered finite structures, comprising both the DBR's and QW's. To complete the picture, the following scattering selection rules have to be justified: (i) the observation of intense peaks originating only from the *upper* DBR-band and QW modes; (ii) the scattering by only one out of every two full cavity DBR modes; (iii) the access to in-plane propagating vibrations in a nearly backscattering configuration; and (iv) the relative intensity of the peaks: in the full cavity the QW and the in-plane DBR mode are the largest, those peaks at the center of the DBR band being relatively weaker. On the other hand, strong suppression occurs for all DBR modes in the test structure.

Point (i) above can be simply understood from symmetry considerations. The modes in the upper (lower) half of Figs. 2 and 4 are mainly polarized along $z(q_\parallel)$. Thus the observation of intense scattering only between the bulk-LO frequency and ≈ 285 cm^{-1} follows from the Raman selection rules for deformation-potential-mediated scattering in crystals belonging to the D_{2d} point group which, for $z'(x,y)\bar{z}$ configuration, correspond to z-polarized $B_2(z)$ symmetry phonons.[15] It is well established, in fact, that deformation-potential scattering dominates in off-resonance light-scattering experiments.[34]

The observation of only one every two modes within the upper DBR band of the AlAs cavity derives from optical-field and phonon-modes symmetries. Since the light field distribution is approximately *even* with respect to the center of the microcavity (see Fig. 1), parity forbids deformation-potential-mediated scattering by modes with *odd* displacement distributions (along z). In fact, consecutive values of q_z correspond to modes of alternating parity. This is demonstrated in Fig. 5, where we show the calculated phonon potentials for some modes of a simplified ''model'' sample with the same structure as the AlAs cavity but, for clarity, a reduced number of DBR layers. The phonon dispersion of this cavity is also shown in Fig. 5 for identification purposes. Solid (dashed) curves were calculated for $q_\parallel = 5(15)\times 10^4$ cm^{-1}. The electrostatic field accompanying a vibration (or equivalently its displacement) can be derived from the potentials shown: its component along $q_\parallel$ is directly proportional to $\phi(z)$, while the z component is proportional to its derivative with respect to z, $\partial\phi(z)/\partial z$, i.e., to the slope of the curves in Fig. 5. Thus potentials which are even with respect to the cavity center correspond to odd z-displacement distributions, and vice versa. For the represented model cavity, the top DBR band reduces to the modes labeled 1 and 2. The former, corresponding to the in-plane propagating vibration of our structure, should be active, while the second mode should be strongly suppressed due to parity. We note here that the continuum dielectric model agrees well with the more sophisticated methods, for GaAs-

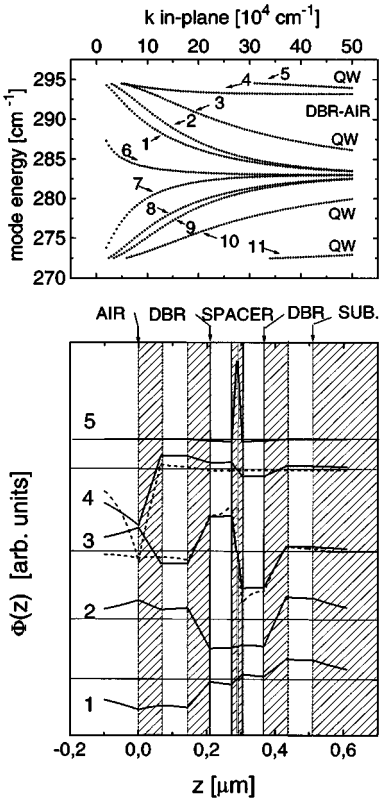

FIG. 5. Top: phonon-mode dispersion corresponding to a model cavity similar to the one used in the experiments but, for clarity, with a reduced number of DBR layers. Bottom: cavity phonon modes associated electrostatic potential $\phi(z)$. The dashed regions represent GaAs layers. The potential represented with solid (dashed) curves corresponds to $q_{\parallel}=5(15)\times10^4$ cm^{-1}.

like vibrations, *only* within the GaAs layers.[18–20] In fact, for GaAs-like modes, mechanical boundary conditions force an almost zero displacement within the AlAs layers, something not reproduced by the curves in Fig. 5.

In Fig. 5 we also present the electrostatic potentials associated with the QW's modes (3 and 5 in Fig. 5, top) and DBR-air surface mode (4 in Fig. 5, top). For $q_{\parallel}=5\times10^4$ cm^{-1} modes (3) and (4) are almost degenerate, resulting in strong mixing. This mixing is lifted for $q_{\parallel}=15\times10^4$ cm^{-1}, a value for which, in addition, much more localized and hence purer ''QW'' and ''surface'' characters are apparent (see the dashed curves in Fig. 5). Due to the parity selection rule outlined above, it can be seen that the doublet structure at the LO-phonon peak (evident in the upper spectrum in Fig. 3) *cannot* come from the two upper QW modes, since the two have opposite parities, the lower one being energy active. Consequently, the smaller peak in the doublet is likely to be due to the ''DBR-air surface mode'' which, as is evident from Fig. 5, for the experimentally transfered $q_{\parallel}\approx5\times10^4$ cm^{-1} is fairly well extended throughout the cavity.

Contrary to the full cavity sample, all phonon modes in the test half-structure scatter (see Fig. 4). We can understand this if we recall that, for this structure, the photon field decays exponentially in the bottom DBR, and hence no parity selection rule holds. This exponential decay also explains the attenuated scattering of the DBR features on the test sample spectrum in Fig. 3.

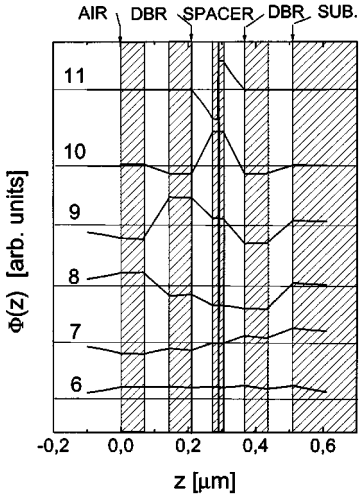

FIG. 6. Electrostatic potential $\phi(z)$ corresponding to modes 6–11 of the model cavity represented in Fig. 5. The potentials were calculated for $q_{\parallel}=5\times10^4$ cm^{-1}.

In Fig. 6 we show the potentials associated with the bottom QW's and DBR-band modes of the model cavity in Fig. 5 (modes 6–11). Comparing Figs. 5 and 6 it follows that, within the GaAs layers, the displacements are mostly z polarized for the upper DBR band, and $q_{\parallel}$ polarized for the lower one. This justifies our previous affirmation that, for the $z'(x,y)\overline{z}$ configuration, scattering occurs mostly from the upper GaAs-like DBR band. Figure 6 also shows that some smaller z component also exists for displacements corresponding to modes in the lower DBR band, as expected for $q_{\parallel}\neq0$.[35] This is most notable for the higher-energy branches of the lower DBR band, thus explaining their observation as weaker features in our spectra (see the open triangles in the topmost spectrum in Fig. 3). The energy of the first structure below the peak at ≈285 cm^{-1} is well described by the calculated phonon dispersion. However, the other weaker peaks do not agree well with the parity selection rule outlined above.

A notable feature in the spectra of Fig. 3 is the observation of strong scattering corresponding to the DBR mode with smallest q_z, i.e., an *in-plane* propagating vibration, something *a priori* in contradiction with the backscattering geometry. Indeed, in the full cavity spectra the latter is as intense as the signal at the bulklike LO frequency. Note, however, that, in a microcavity, photons are multiply reflected due to the DBR's. Thus we can understand the observed effect as due to forward-scattering processes which are present for backscattering experiments performed on the face normal to z in microcavity structures.

A detailed description of the relative intensity of each peak contributing to the spectra [point (iv) above] may only be possible after a calculation of the respective Raman efficiencies is performed. However, some insight can be gained by analyzing the wave vector transfered in the scattering process. In fact, although the z wave vector component is not strictly conserved due to the lack of full periodicity, *partial* conservation[28] may be expected for the DBR modes. The transfered q_z, under this latter assumption, depends on whether the process of excitations is through forward or

backward scattering. For the former, $\vec{q}$ is mainly perpendicular to z (i.e., $q_z \approx 0$), while for the latter it is mostly along z.[15]

The Raman signal can thus be separated into two contributions coming from forward and backward scattering, respectively. Both couple to the QW's modes, which are independent of q_z, leading to scattering close to the bulk-LO frequency (≈ 295 cm^{-1}). Concerning the DBR's, forward scattering couples to the bottommost branch of the upper band (≈ 285 cm^{-1}, full square in Fig. 2), which corresponds to a discretized $q_z \approx 0$. The backscattering contribution, on the other hand, may only be derived after some guess regarding the magnitude of q_z is made.

If the scattering proceeds for GaAs-like vibrations mainly at the GaAs layers, then $q_z \approx 2\pi n_{\mathrm{GaAs}}/\lambda$, where n_{GaAs} is the GaAs refractive index and λ the laser wavelength in vacuum. This should occur for deformation-potential-mediated scattering if the displacements are confined to the GaAs layers. In this case, coupling should be more intense for those modes with discretized q_z closest to $q_z \approx 2\pi n_{\mathrm{GaAs}}/\lambda$.[28] To decide which modes these are, one has simply to calculate the interface-phonon dispersion for an *infinite* DBR corresponding to that q_z. We find that this curve crosses the experimental $q_\parallel$ at ≈ 289 cm^{-1}, where indeed the most intense secondary peaks are observed.

Note that in Ref. 11 we used an average refrective index for the heterostructure, i.e., we considered the scattering process extended throughout both GaAs and AlAs layers. In this case, by construction, for the cavity double resonance q_z is exactly $2\pi/d$,[11] which for an infinite layered structure is equivalent to zero.[1] Thus, if an ''average medium'' picture applies, the backscattering contribution should coincide with that coming from forward scattering, i.e., scattering should occur for the mode at ≈ 285 cm^{-1}. Within this approach one has to find another explanation for the observation of the secondary peaks between the LO frequency and ≈ 285 cm^{-1}. The most natural explanation relies on assuming q_z partial nonconservation due to the lack of full periodicty. However, q_z nonconservation should lead in this case to a distribution of wave vectors centered at $q_z = 0$, and thus the spectral weight should be displaced toward the lower part of the DBR's upper band, in contradiciton with the experiment.

C. In-plane dispersion

The geometrical conditions required for optical double resonance in planar microcavities can be attained under a continuum of collection and (correspondingly fixed) incidence angles. Thus the transferred wave vector $q_\parallel$ can be varied, giving access to part of the excitations' in-plane dispersion. In this subsection we present a study of the phonon dispersion performed on the second group of samples described in Sec. III, i.e., the MQW and test-MQW cavities. Besides providing a complementary test of our mode assignment, these samples are comparatively simpler (and interesting) in that the GaAs-like phonon modes related to the DBR's (made of AlAs and an $Al_xGa_{1-x}As$ alloy) are spectrally shifted from those of the material making the spacer, that is, the GaAs/AlAs MQW. Being the spacer completely filled by the active material, the Raman signals are also more intense and thus experiments in the half-cavity test structures

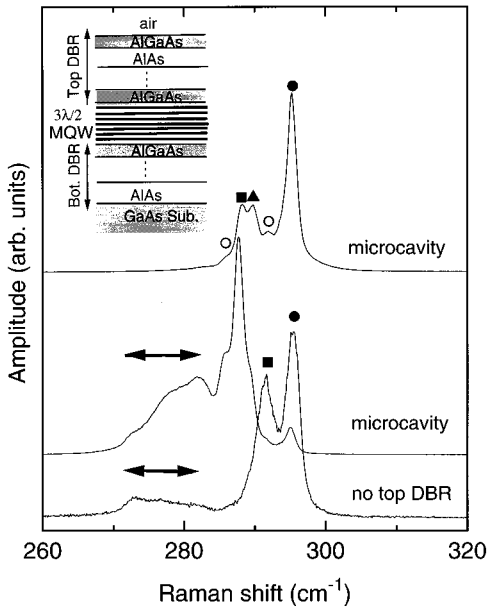

FIG. 7. GaAs-like optical-phonon Raman spectra taken with the $z'(x,y)\bar{z}$ configuration for both the MQW cavity and test (without top DBR) samples. The laser energy is 1.44 eV, incident at 52° with respect to z (external to the sample). Stokes photons are collected along z. θ_0 was tuned for cavity optical double resonance between the LO peak ≈ 295 cm^{-1} and that at ≈ 287 cm^{-1}. The two MQW-cavity spectra (top curves) correspond to different spot positions on the wafer, i.e., selective enhancement of different Stokes regions. A sketch of the cavity sample is shown as an inset.

can be more easily performed. Furthermore, as we will discuss in Sec. IV D, scattering by folded acoustic phonons can be also studied.

In Fig. 7 we show GaAs-like optical-phonon spectra taken with laser excitation at 1.44 eV (well below the MQW gap, ≈ 1.6 eV) and an incidence angle of 52° (the collection, as before, was done along z). As for the previously described samples, these spectra were only observed under a crossed $z'(x,y)\bar{z}$ configuration. We show spectra for both the test sample and the full cavity structure, the latter taken at two slightly different spot positions (hence selectively enhancing different parts of the spectra). Two regions can be differentiated, one (always stronger) between the GaAs bulklike LO frequency (295 cm^{-1}) and ≈ 287 cm^{-1}, where clear peaks appear, and a second broader and almost featureless between ≈ 282 and ≈ 272 cm^{-1}. We will demonstrate below that the former is mainly due to MQW vibrations, while the latter corresponds to $Al_xGa_{1-x}As$ phonons in the DBR's. The MQW contribution to the spectra consists basically on two large peaks, labeled in Fig. 7 with solid circles and squares, respectively, with in addition some secondary features. This resembles the results on the AlAs cavity (see Fig. 3), where again two peaks, one at the LO frequency and the other corresponding to an in-plane propagating mode, dominated the spectra. As for the AlAs cavities, the spectral position of the lower energy peak (full squares in Fig. 7) does not coincide for the cavity and test samples, being clearly shifted toward larger frequencies for the half-structure.

In Figs. 8 and 9 we present the calculated interface phonon dispersion for these two structures. As before, there are

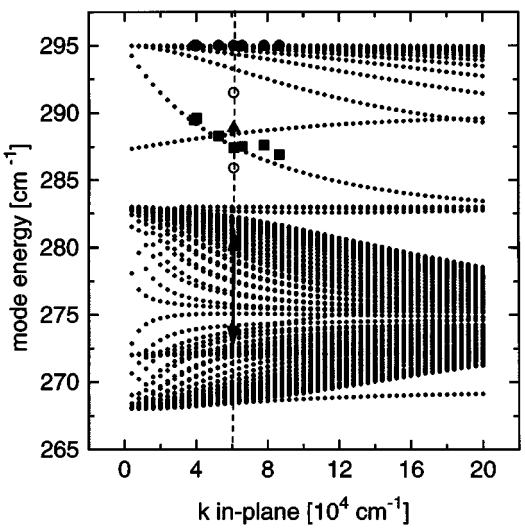

FIG. 8. Calculated MQW-cavity heterostructure interface-phonon dispersion (small dots) as a function of in-plane wave vector $q_\parallel$. The vertical dashed line denotes the experimental transferred $q_\parallel$. The same symbols are used to label the experimental points and the corresponding peaks in Fig. 7.

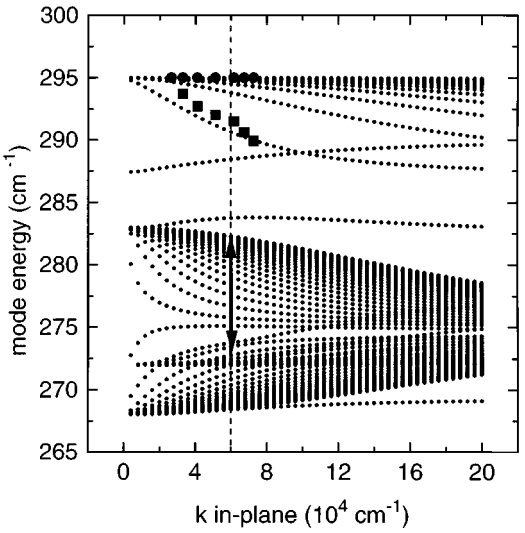

FIG. 9. Calculated test-MQW sample interface-phonon dispersion (small dots) as a function of in-plane wave vector $q_\parallel$. The vertical dashed line denotes the experimental transferred $q_\parallel$. The same symbols are used to label the experimental points and the corresponding peaks in Figs. 7 and 10.

no fitting parameters: the GaAs, $Al_xGa_{1-x}As$, and AlAs phonon frequencies are taken from the literature,[31] and nominal layer thicknesses are used. For the GaAs-like modes of the $Al_{0.33}Ga_{0.67}As$ alloy making the mirrors, we used $LO_{Al_xGa_{1-x}As}=282.5\ cm^{-1}$ and $TO_{Al_xGa_{1-x}As}=268\ cm^{-1}$. The phonon dispersions can be understood basically as a superposition of the separate contributions of the DBR's and the MQW. Each contributes a top and a bottom band of discretized modes going from their LO and TO frequencies, respectively, to approximately the midfrequency between them. However, two distinct features signal some coupling between these two types of vibrations, originating in the long-range character of the Coulomb interaction and on the fact that the optical modes of the MQW and DBR's are *not* completely separated in energy. First, the bottommost mode of the upper MQW band strongly shifts in the half-cavity as compared to the full one. The fact that this mode is not equal for the two samples where the MQW is exactly the same indicates that the smallest quantized q_z is not only determined by the thickness of the MQW, but is also influenced by the presence of the DBR's surrounding it. Second, and related to the same delocalization of interface vibrations, a mode in the LO-like MQW spectral region develops an *upward* dispersion with increasing $q_\parallel$. An effect similar to the latter was already reported in Ref. 36.

Experimental points taken from Fig. 7 are shown for comparison together with the calculated dispersions in Figs. 8 and 9. For clarity, the same symbols are used to label the peaks in all figures. The following conclusions can be drawn: (i) Scattering occurs principally at the upper MQW and DBR bands, as expected from deformation-potential-mediated scattering by phonons of $B_2(z)$ symmetry.[15] (ii) The finite-size effect determining the smallest q_z provides a natural explanation for (and quantitatively reproduces) the difference of frequency of the in-plane propagating modes in the two studied structures (full squares). (iii) The weaker peak at the higher-energy side of the full cavity in-plane interface mode (labeled with a solid triangle) may be assigned to the upward dispersing mode. (iv) Finally, the weak structures appearing for the MQW full cavity between the LO and in-plane modes, and below the latter (open circles in Figs. 7 and 8), cannot be accounted for by the simple dielectric continuum model discussed here. These two small structures could be due to higher-order MQW confined modes. In fact, for the relatively thin layers making the MQW, the dielectric continuum model well describes the anisotropic behavior of the first-order confined mode,[29] but fails to include the higher-order confined vibrations which can only be properly described by also considering mechanical boundary conditons and the wave-vector dependence of the bulk-phonon dispersion.[18]

In the AlAs cavities described above, the in-plane propagating vibration corresponds to a DBR mode which is consequently strongly attenuated in the test sample spectra. This contrasts with the MQW sample presented here: the observed in-plane interface mode is mostly a MQW vibration, thus explaining its large amplitude even in the half-structure. This fact, together with the relative simplicity of the spectra, make the MQW cavities good candidates to study in-plane dispersions. In Fig. 10 we show spectra for the test-MQW half-cavity taken with different incident angles and collection along z. The LO-frequency vibration stays dispersionless, while the contrary holds for the in-plane mode. These data are plotted in Fig. 9 together with the calculated dispersions: excellent accord with theory is found.

The study of in-plane dispersions for the full cavity is, however, somewhat more complicated in that the high finesse of the structure requires a precise tuning of both excitation and collection angles to observe any signal.[11] We found that this was most conveniently done in an anti-Stokes configuration. For the latter, light is collected at a large angle, and the possible excitations directions, according to

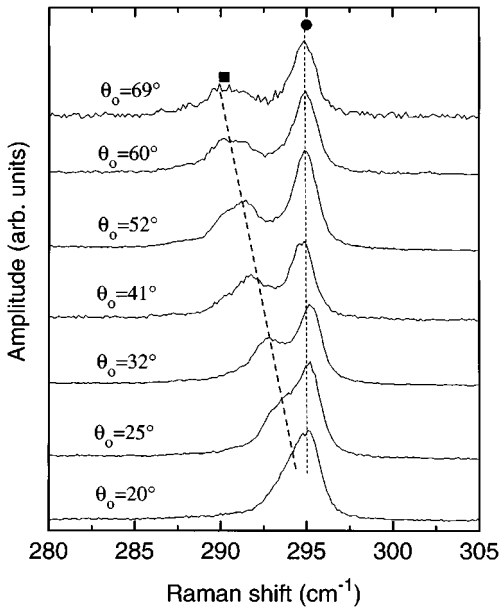

FIG. 10. GaAs-like optical-phonon Raman spectra taken with the $z'(x,y)\bar{z}$ configuration for the test-MQW half-cavity. Stokes photons are collected along z. The laser energy is 1.44 eV, incident at different angles (θ_o) to vary the transfered $q_\parallel$. The lines are guides to the eye.

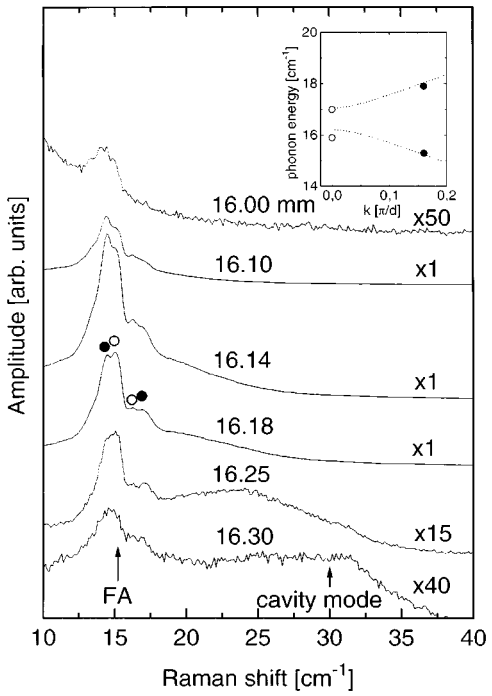

FIG. 11. MQW-cavity folded-acoustic (FA)-phonon Raman spectra taken with parallel configuration. The laser energy is 1.44 eV, incident at 20° respect to z (external to the sample), for optical double resonance at the first FA-phonon doublet. Stokes photons are collected along z. The spectra correspond to several spot position on the wafer, i.e., different optical-resonance detunings. Exact double resonance is obtained when the cavity mode along z (visible in the figure due to residual luminescence) coincides with the FA-phonon Stokes energy. Note a *doubling* of the usual FA-phonon doublet, signaling the presence of both forward-scattering and backscattering processes due to multiple reflections at the DBR's. The experimental peaks are compared in the inset with the calculated mode dispersions. d corresponds to the MQW's period.

Eq. (1), define a cone of smaller angle around the z axis. Hence, two different $q_\parallel$'s can be easily probed on incidence at two symmetric directions close to the z axis. In this way we followed the $q_\parallel$ dependence of the two larger peaks in the spectra, represented with full squares in Fig. 8 together with the calculated curves. Again the results are very well accounted for by theory, supporting our assignment. We recall that in-plane vibrations in cavity structures are accessible through forward-scattering processes allowed by the presence of the mirrors. In fact, as shown in Fig. 10, the simple inclusion of the bottom mirror is an interesting alternative to study in-plane dispersions and forward-scattering processes.[37]

D. Folded acoustic-phonon scattering

Before finishing the presentation of our data, let us briefly discuss folded acoustic-phonon scattering performed in the MQW-cavity structure. Although somewhat different to the interface optical vibrations described up to here, these results provide a complementary demonstration of the existence of forward-scattering processes in backscattering geometries performed in cavity structures. Furthermore, they provide an example of easily recognizable excitations which can be used to monitor the field distribution in these photonic structures.

In Fig. 11, we show MQW-cavity spectra taken for different spot positions (i.e., different cavity detunings) and with an incidence angle ($\approx 20°$) appropriate for a double resonance at the first folded acoustic-phonon pair. The amplifying capabilities of a microcavity, already demonstrated for optical vibrations in Ref. 11, are shown: the largest scattering efficiency is obtained on tuning to an optical double resonance of these high-finesse cavities. This double resonance corresponds to the position in the wafer for which the cavity mode (observable in Fig. 11 due to residual luminescence) coincides with the folded acoustic (FA)-phonon Stokes energy. By displacing only some tenths of a millimeter away the spot position, the FA-phonon signal becomes unobservable. We note also that, under the same experimental conditions (laser power, wavelength, temperature, and geometry), we were not able to observe any scattering by folded acoustic phonons in a 3-μm-thick MQW directly grown on GaAs, i.e. without DBR mirrors.

The observation of Raman scattering by $q \approx 0$ acoustic modes in MQW's derives from the folding of the phonon dispersions introduced by the layering generated reduction of the Brillouin zone. Thus the position of these Raman peaks depends only on the MQW's period. In general, doublets are observed and not single peaks, due to the opening of gaps at zone center and edge.[1] Most interestingly, Fig. 11 shows that in a microcavity these typical folded-acoustic-phonon doublets are themselves *doubled*. The observed doubling can be easily understood as due to the different $q_\parallel$'s transferred in backscattering and forward-scattering processes. A quantitative check of this assignement is given in the inset of Fig. 11,

where the peak positions are compared with the calculated folded-acoustic-phonon dispersion.

V. CONCLUSIONS

We have presented a detailed and comprehensive study of phonon Raman scattering in semiconductor planar microcavities. GaAs-like optical-phonon scattering originating from the ''interface-phonon'' band of these layered structures was reported. These modes are discretized by finite-size effects, leading to complex spectra with several peaks. Besides the symmetry-based Raman selection rules that predict scattering only from z-polarized vibrations, we have shown that a parity selection rule exists which forbids the coupling of modes with odd (respect to the center of the cavity) z-displacement distribution. By varying the incidence and collection angles, the vibration's in-plane dispersion was also derived. The energies of the observed modes can be well accounted for by a continuum dielectric model. The various peaks in the spectra correspond to phonons characterized by displacements with different spatial distribution. Thus a calculation of the Raman spectra may provide valuable information regarding the field distribution within these photonic structures. A proper cavity design, e.g., by using different materials in the mirrors and spacer, or by looking at specific excitations as, for example, folded acoustic phonons, can also be exploited for this purpose. Finally, a doubling of the folded-acoustic-phonon doublet in a MQW embedded microcavity was observed, signaling the presence of forward scattering in addition to backscattering processes in cavity structures.

ACKNOWLEDGMENTS

We are pleased to aknowledge I. Abram, J. I. Bloch, G. Le Roux, J. Y. Marzin, J. L. Oudar, and R. Planel for numerous helpful discussions. Special thanks are also due to P. Etchegoin (Cavendish Lab., Cambridge, U. K.) for valuable comments on the manuscript, and to V. Thierry-Mieg for providing us the samples used in this work. A.F. thanks the Consejo Nacional de Investigaciones Científicas y Técnicas de la República Argentina for support.

[1] B. Jusserand and M. Cardona, in *Light Scattering in Solids*, edited by M. Cardona and G. Güntherodt (Springer, Berlin, 1989), Vol. 5; D. L. Mills, *ibid*; A. Pinczuk and G. Abstreiter, *ibid*.

[2] José Menéndez, J. Lumin. **44**, 285 (1989).

[3] See, for instance, *Cavity Quantum Electrodynamics*, edited by P. R. Berman (Academic, Boston, 1994).

[4] For a review, see Y. Yamamoto and R. E. Slusher, Phys. Today **46**(6), 66 (1993); R. E. Slusher and C. Weisbuch, Solid State Commun. **92**, 149 (1994).

[5] K. H. Drexhage, J. Lumin. **1,2**, 693 (1970); K. H. Tews, *ibid.* **9**, 223 (1974); R. R. Chance, A. Prock, and R. Silbey, in *Advances in Chemical Physics*, edited by I. Prigogine and S. A. Rice (Wiley, New York, 1978), pp. 1–65.

[6] E. Yablonovitch, Phys. Rev. Lett. **58**, 2059 (1987).

[7] F. De Martini *et al.*, Opt. Lett. **17**, 1370 (1992).

[8] G. A. N. Connell, R. J. Nemanich, and C. C. Tsai, Appl. Phys. Lett. **36**, 31 (1980); R. J. Nemanich, C. C. Tsai, M. J. Thompson, and T. W. Sigmon, J. Vac. Sci. Technol. **19**, 685 (1981).

[9] H. Metiu, Prog. Surf. Sci. **17**, 153 (1982).

[10] F. Cairo, F. De Martini, and D. Murra, Phys. Rev. Lett. **70**, 1413 (1993).

[11] A. Fainstein, B. Jusserand, and V. Thierry-Mieg, Phys. Rev. Lett. **75**, 3764 (1995).

[12] A. Fainstein, B. Jusserand, and V. Thierry-Mieg, Phys. Rev. B **53**, R13 287 (1996).

[13] R. P. Stanley, R. Houdré, U. Oesterle, M. Ilegems, and C. Weisbuch, Phys. Rev. A **48**, 2246 (1993).

[14] A. Yariv and P. Yeh, *Optical Waves in Crystals* (Wiley, New York, 1984).

[15] M. Cardona, in *Light Scattering in Solids*, edited by M. Cardona and G. Güntherodt (Springer, Berlin, 1982), Vol. 2.

[16] A. Otto, in *Light Scattering in Solids*, edited by M. Cardona and G. Güntherodt (Springer, Berlin, 1984), Vol. 4.

[17] See, for instance, K. Huang and B. Zhu, Phys. Rev. B **38**, 13 377 (1988).

[18] For a clear almost tutorial presentation of the hybrid electrostatic-hydrodynamical models, see R. Pérez-Alvarez, F. Garcia Moliner, V. R. Velasco, and C. Trallero-Giner, J. Phys. Condens. Matter **5**, 5389 (1993). See also M. P. Chamberlain, M. Cardona, and B. K. Ridley, Phys. Rev. B **48**, 14 356 (1993), and references therein.

[19] E. Richter and D. Strauch, Solid State Commun. **64**, 867 (1987).

[20] S. Baroni, P. Giannozi, and E. Molinari, Phys. Rev. B **41**, 3870 (1990).

[21] D. J. Evans, S. Ushioda, and J. D. McMullen, Phys. Rev. Lett. **31**, 369 (1973).

[22] M. Nakayama, M. Ishida, and N. Sano, Phys. Rev. B **38**, 6348 (1988).

[23] R. E. Camley and D. L. Mills, Phys. Rev. B **29**, 1695 (1984).

[24] B. L. Johnson, J. T. Weiler, and R. E. Camley, Phys. Rev. B **32**, 6544 (1985).

[25] P. Hawrylak, G. Eliasson, and J. J. Quinn, Phys. Rev. B **34**, 5368 (1986).

[26] J. K. Jain and P. B. Allen, Phys. Rev. Lett. **54**, 947 (1985); **54**, 2437 (1985).

[27] G. Eliasson, P. Hawrylak, and J. J. Quinn, Phys. Rev. B **35**, 5569 (1987).

[28] A. Pinczuk, M. G. Lamont, and A. C. Gossard, Phys. Rev. Lett. **56**, 2092 (1986).

[29] It should be noted that this distinction between ''confined'' and ''interface'' modes does not apply when more elaborate models are used. In fact, in the latter, the interface modes we describe here correspond to the first-order confined vibrations which, due to their larger macroscopic electric field, display a marked anisotropy as a function of propagation angle.

[30] The Rabi splitting and guiding properties of this structure were reported by I. Abram, S. Iung, R. Kuszelewics, G. Le Roux, C. Licoppe, J. L. Oudar, J. I. Bloch, R. Planel, and V. Thierry-Mieg, Appl. Phys. Lett. **65**, 2516 (1994).

[31] B. Jusserand, in *Properties of Aluminium Gallium Arsenide*, edited by S. Adachi (IEE, London, 1993).

[32] See, for instance, F. Iikawa, F. Cerdeira, C. Vazquez-Lopez, P. Motisuke, M. A. Sacilotti, A. P. Roth, and R. A. Masut, Solid State Commun. **68**, 211 (1988).
[33] S. de Gironcoli, Phys. Rev. B **46**, 2412 (1992).
[34] A. K. Sood, J. Menendez, M. Cardona, and K. Ploog, Phys. Rev. Lett. **54**, 2111 (1985).
[35] A. Fainstein, P. Etchegoin, M. P. Chamberlain, M. Cardona, K. Tötenmeyer, and K. Eberl, Phys. Rev. B **51**, 14 448 (1995).
[36] L. G. Quagliano, B. Jusserand, D. Orani, M. R. Bruni, and M. G. Simeone, Solid-State Electron. (to be published).
[37] B. Jusserand, F. Alexandre, J. Dubard, and D. Paquet, Phys. Rev. B **33**, 2897 (1986).